IL NUOVO CIMENTO **46 C** (2023) 60
DOI 10.1393/ncc/i2023-23060-7

COMMUNICATIONS: SIF Congress 2022

Top-quark pair cross-section at $\sqrt{s} = 13.6$ TeV with the ATLAS experiment

L. PINTUCCI(*) on behalf of the ATLAS COLLABORATION
INFN Sezione di Trieste, Università degli Studi di Udine - Udine, Italy

received 31 January 2023

Summary. — The ATLAS detector started collecting data in 2022 at the centre-of-mass energy $\sqrt{s} = 13.6$ TeV. In this report, an analysis of proton-proton collision data collected in August 2022 by the ATLAS detector at the LHC is shown. The analysis aim is to measure the top-quark pair production cross-section and its ratio to the Z boson production cross-section. Some of the first plots showing a comparison between Run 3 data and predictions in the $e\mu$ final state are presented.

1. – Introduction

Since July 2022 the Large Hadron Collider (LHC) [1] at CERN has restarted its operation, collecting data at the record centre-of-mass energy of $\sqrt{s} = 13.6$ TeV during what is called Run 3. The ATLAS detector [2] and reconstruction software went through various upgrades, before the start of the new data-taking period. It is therefore important to perform early data analyses, using data collected at the new centre-of-mass energy, in order to find possible issues and to validate the new experimental setup.

The ATLAS experiment has measured the top-quark pair ($t\bar{t}$) production cross-section, as well as the Z-boson production cross-section, at different centre-of-mass energies $\sqrt{s} = 7, 8$, and 13 TeV [3-8]. These measurements are excellent tests of electroweak (EW) and quantum chromodynamics (QCD) processes at the LHC. The precision reached in such measurements is of the order of a few percent in the $t\bar{t}$ case, sub-percent for the Z production process. Theoretical predictions are available at the next-to-next-to-leading-order (NNLO) accuracy in the strong coupling constant α_s for the $t\bar{t}$ inclusive cross-section [9], and at the NNLO QCD plus next-to-leading-order (NLO) EW accuracy for the Z production cross-section [10]. A comparison between measurements and predictions can be used to constrain fundamental parameters of the Standard Model (SM),

(*) E-mail: laura.pintucci@cern.ch

as α_s, or the top-quark mass (m_t). Ratios between the $t\bar{t}$ and Z cross-sections have also been measured at the previously mentioned centre-of-mass energies [11].

2. – Data and Monte Carlo samples

This analysis uses data from proton-proton (pp) collisions collected by the ATLAS experiment at an energy in the centre-of-mass of 13.6 TeV between the 6th and the 22nd of August 2022. Some data quality requirements are applied to this data to ensure they are free from any hardware or software-related issues [12], and it results in an integrated luminosity of $L = 790\,\text{pb}^{-1}$.

In this analysis, all simulated datasets are created with a full Monte Carlo (MC) simulation of final states of pp collisions, produced through SM processes, and interacting with the ATLAS detector. The interaction between particles and the detector is simulated with GEANT4 [13]. All the MC samples are generated considering the top quark mass to be $m_t = 172.5\,\text{GeV}$.

The $t\bar{t}$ MC sample is produced with Powheg Box v2 [14, 15], interfaced to Pythia 8.307 [16], with the A14 set of tunable parameters [17]. Top++ 2.0 [18] is used to compute the SM $t\bar{t}$ cross-section prediction at NNLO in QCD, with resummation of next-to-next-to-leading logarithmic (NNLL) soft-gluon terms. The Z boson sample is generated with Powheg Box v2 interfaced with Pythia 8.307, using the AZNLO tune [19]. Single top tW, t-channel, and s-channel samples are simulated with Powheg Box v2 at NLO in QCD using the five-flavour scheme (four-flavour scheme for the t-channel process) interfaced with Pythia 8.307, with the A14 set of tunable parameters. In the case of the tW sample, the diagram removal scheme [20] is used to remove overlap and interference with the $t\bar{t}$ sample. The $W + jets$ sample is simulated using Sherpa 2.2.12 [21], the events are normalized at NNLO in QCD and with NLO EW corrections using MATRIX software [22]. Diboson samples (VV) are also produced with Sherpa 2.2.12, considering fully leptonic and semi-leptonic final states with matrix elements at NLO (leading order (LO)) for up to one (three) additional parton emissions.

3. – Analysis strategy and event selection

3˙1. *Analysis strategy.* – This analysis aims at studying the $t\bar{t}$ production, as to obtain its cross-section measurement $\sigma_{t\bar{t}}$ at the centre-of-mass energy of $\sqrt{s} = 13.6\,\text{TeV}$.

At LO the $t\bar{t}$ pair can be produced via three Feynman diagrams, shown in fig. 1. The top quark pair can then decay in three different ways: in the dilepton channel $pp \to t\bar{t} \to W^-\bar{b}W^+b \to b\bar{b}l^+l^-\nu_l\bar{\nu}_l$, in the semi-leptonic channel $pp \to t\bar{t} \to W^-\bar{b}W^+b \to b\bar{b}l\nu_l jj$, and in the fully hadronic channel $pp \to t\bar{t} \to W^-\bar{b}W^+b \to b\bar{b}jjjj$.

In comparison with the other decay channels, the measurement of the $t\bar{t}$ production cross-section in the dilepton channel does not depend strongly on jet-related quantities and therefore it is easier to be considered when using data samples obtained with the new experimental setup for Run 3. Data considered in this analysis have an associated luminosity uncertainty of 10%, which would be by far the main uncertainty in the cross-section measurement. In order to have a more precise measurement one can consider the ratio between the $t\bar{t}$ production cross-section in the dilepton channel and the Z production cross-section. When measuring this ratio, the luminosity uncertainty on the $t\bar{t}$ and Z measurements cancels out.

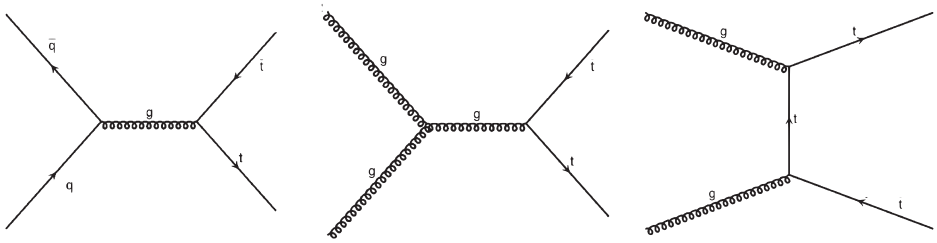

Fig. 1. – Feynman diagrams at LO of top quark pair production from proton-proton collisions.

3˙2. *Object definition.* – Events are selected using single electron or single muon triggers. Moreover, events are required to have two or more tracks with $p_T > 500$ MeV associated with one collision vertex.

Electron candidates are reconstructed from the matching of an electromagnetic cluster in the electromagnetic (EM) calorimeter with a particle track in the Inner Detector (ID). Electron candidates are required to have a transverse momentum p_T greater than 27 GeV, an absolute value of the pseudorapidity $|\eta| < 2.37$ and to be outside the transition region $1.37 < |\eta| < 1.52$, and they need to fulfil *TightLH* identification criteria and *Tight* isolation criteria as defined in [23]. Scale Factors (SFs) to match reconstruction, identification, isolation, and trigger MC efficiencies to data have been computed. Electron identification SFs are computed using Run 2 data with the Run 3 reconstruction software, while other electron SFs are assumed to be one.

Muon candidates are reconstructed by matching tracks in the Muon Spectrometer (MS) to tracks in the ID. Muon candidates are required to have $p_T > 27$ GeV, $|\eta| < 2.5$, and need to fulfill *MediumLH* identification criteria and *Tight* isolation criteria, as defined in [24]. Identification, isolation, reconstruction, and trigger SFs for muons have been computed using Run 3 data.

Jet candidates are reconstructed with the anti-k_t jet algorithm [25] from clusters of topologically connected calorimeter cells, using a jet radius parameter $R = 0.4$. Candidate jets are calibrated with the *Particle Flow* algorithm [26]. These jets are then required to have $p_T > 30$ GeV, $|\eta| < 2.5$, and they need to fulfil the *JVTTight* working point requirements on the Jet Vertex Tagger (JVT) [27]. Jets originating from a b quark (b-jet) are selected with the DL1D algorithm, which is based on a Deep Neural Network (DNN) similar as defined in [28]. The DNN outputs three values, which represent the probability of the jet coming from a light quark (light-tag), a c quark (c-tag), or a b quark (b-tag). The efficiency working point used to tag a jet as a candidate b-jet is 77%.

3˙3. *Event selection.* – Events are selected if they contain two leptons of opposite charge. Events with one electron and one muon ($e\mu$) are required to have at least one jet, and at least one b-jet. Events with same flavour leptons (ee, $\mu\mu$) are required to have a dilepton invariant mass in the so-called *Z mass window* $76\,\text{GeV} < m_{ll} < 106\,\text{GeV}$.

The fit strategy is to use the *b-tag counting method* [29] in the $e\mu$ region to extract the $t\bar{t}$ cross-section. This method counts the number of events in two bins: N_1 is the number of events with one b-jet, and N_2 is the number of events with two b-jets. Then a Profile Likelihood fit is used in three different regions ee, $\mu\mu$, and $e\mu$ to extract the $t\bar{t}$ over Z cross-section ratio.

4. – Systematic uncertainties

The main uncertainty in this analysis is the one on the luminosity of the data collected during August 2022. It is estimated to be of 10% as a conservative uncertainty, considering the upgrade to the LUCID2 [30] detector and the long shutdown 2 that lasted 4 years, during which the LHC operation was stopped.

Electron energy corrections are estimated from Run 2 as in [23], and their uncertainties are inflated based on differences in the reconstruction between Run 2 and Run 3 estimated on MC simulations. Uncertainties related to electron identification SFs are computed similarly to [23, 31], with some additional uncertainties obtained comparing MC simulations between Run 2 and Run 3. As indicated above, reconstruction, isolation, and trigger electron SFs are assumed to be one. Uncertainties on the isolation and reconstruction SFs are computed as the difference between one and Run 2 SFs. A dedicated study has been performed using Run 3 data to compute electron trigger SFs using the Tag and Probe method. The difference between one and the SFs obtained in this study is considered as an uncertainty in the electron trigger SF.

Muon momentum corrections are estimated from Run 2 calibration, similarly to [24], with inflated uncertainties that cover the difference between Run 2 and Run 3. Uncertainties on muon SFs are computed using the Tag and Probe method with Run 3 data as described here [32].

Uncertainties on Jet Energy Scale (JES) [33], Jet Energy Resolution (JER) [34] and on the jet-vertex-tagging are estimated in Run 2, with additional inflated uncertainties obtained by comparing Run 2 and Run 3 MC simulations. Conservative uncertainties related to the b-tagging of jets are assigned as: 10% uncertainty on the b-efficiency, 20% on the c-mis-tag efficiency, and 40% on the light-flavor-mis-tag.

Modelling uncertainties on the $t\bar{t}$ MC sample are considered both for the shower and the hadronization process. They are estimated comparing MC samples generated with POWHEG + PYTHIA8 and POWHEG + HERWIG7. Moreover, an uncertainty estimated by varying the h_{damp} parameter between $1.5 \cdot m_{top}$ and $3 \cdot m_{top}$ is considered. A 50% normalization uncertainty is applied to Z+jets, diboson, and lepton fakes MC samples, while a 5.3% normalization uncertainty is used for the tW sample.

5. – Results

Using the event selection described in **3**˙3 for the opposite flavour ($e\mu$) region, some distributions showing a comparison of data to MC predictions are shown in the following.

In fig. 2 electron p_T and η distributions are presented. They show a good agreement between data and MC within the considered uncertainties. In fig. 3 muon p_T and η distributions are presented. Similarly to the electron distributions, a good agreement between data and MC predictions is found.

Finally, the distribution of the b-tagged jet multiplicity for the DL1D tagger algorithm is shown in fig. 4. The ratio between data and MC predictions is consistent with one in every histogram bin, considering systematic uncertainties. These plots are an important input to validate the functionality of the reconstruction software and detector after the upgrades realized before the start of Run 3.

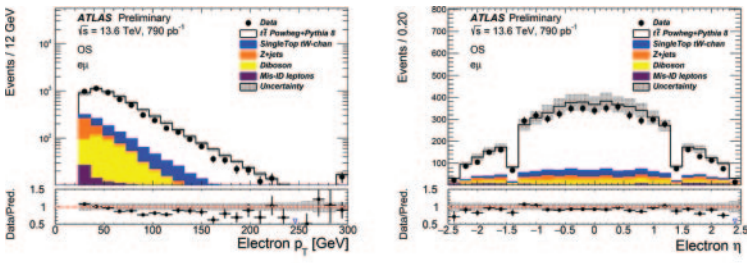

(a) (b)

Fig. 2. – Distribution of the electron p_T (a) and electron η (b) in events selected with an opposite sign $e\mu$ pair. In both plots the top panel shows a comparison of data to MC predictions, while the bottom panel shows the ratio between data and MC in each histogram bin [35].

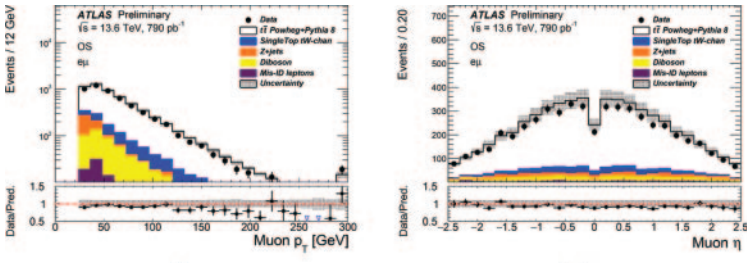

(a) (b)

Fig. 3. – Distribution of the muon p_T (a) and muon η (b) in events selected with an opposite sign $e\mu$ pair. In both plots the top panel shows a comparison of data to MC predictions, while the bottom panel shows the ratio between data and MC in each histogram bin [35].

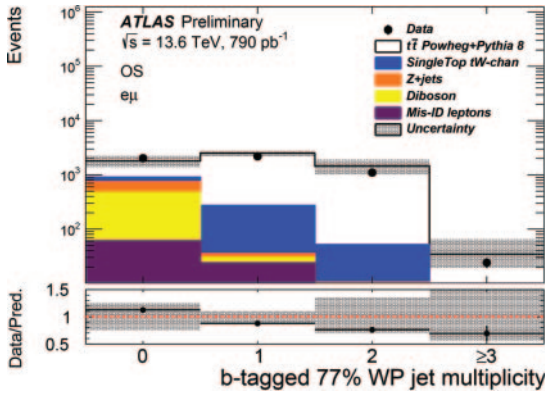

Fig. 4. – Distribution of the b-tagged jet multiplicity for the DL1D tagger algorithm with a 77% working point, in events selected with an opposite sign $e\mu$ pair. The top panel shows a comparison of data to MC predictions, while the bottom panel shows the ratio between data and MC in each histogram bin [35].

6. – Conclusions

In this work, an analysis of proton-proton collision data collected in August 2022 with the ATLAS experiment at the LHC has been described. This analysis aims to extract the

$t\bar{t}$ production cross-section, and its ratio with the Z cross-section in the dilepton decay channel. Data used in this analysis are the first data collected at the beginning of Run 3 operation at a centre-of-mass energy of $\sqrt{s} = 13.6\,\text{TeV}$ at LHC and used in an ATLAS physics analysis. Run-3 operation resumed in 2022 after a long shutdown of four years, during which the ATLAS experiment and software were updated. In this report, some of the first plots showing a comparison between Run-3 data and predictions in the $e\mu$ final state are presented. As can be seen in such plots, there is a good agreement between data and MC, and they agree within the estimated uncertainties.

REFERENCES

[1] Evans L. and Bryant P., *JINST*, **3** (2008) S08001.
[2] ATLAS Collaboration, *JINST*, **3** (2008) S08003.
[3] ATLAS Collaboration, *Eur. Phys. J. C*, **74** (2014) 3109 (Addendum: *Eur. Phys. J. C* 76 (2016) 642).
[4] ATLAS Collaboration, *Phys. Lett. B*, **711** (2012) 244.
[5] ATLAS Collaboration, *Eur. Phys. J. C*, **80** (2020) 528.
[6] ATLAS Collaboration, *Phys. Rev. D*, **85** (2012) 072004.
[7] ATLAS Collaboration, *Eur. Phys. J. C*, **76** (2016) 291.
[8] ATLAS Collaboration, *Phys. Lett. B*, **759** (2016) 601.
[9] Cacciari M., Czakon M., Mangano M., Mitov A. and Nason P., *Phys. Lett. B* , **710** (2012) 612.
[10] Catani S. and Grazzini M., *Phys. Rev. Lett.*, **98** (2007) 222002.
[11] ATLAS Collaboration, *JHEP*, **02** (2017) 117.
[12] ATLAS Collaboration, *JINST*, **15** (2020) P04003.
[13] Agostinelli S. *et al.*, *Nucl. Instrum. Methods A*, **506** (2003) 250.
[14] Frixione S., Nason P. and Ridolfi G., *JHEP*, **09** (2007) 126.
[15] Alioli S., Nason P., Oleari C. and Re E., *JHEP*, **06** (2010) 043.
[16] Bierlich C. *et al.*, *SciPost Phys. Codebases 8-r8.3* (2022).
[17] ATLAS Collaboration, ATL-PHYS-PUB-2014-021 (2014) `https://cds.cern.ch/record/1966419`.
[18] Czakon M. and Mitov A., *Comput. Phys. Commun.*, **185** (2014) 2930.
[19] ATLAS Collaboration, *JHEP*, **09** (2014) 145.
[20] Frixione S., Laenen E., Motylinski P., Webber B. R. and White C. D., *JHEP*, **07** (2008) 029.
[21] Bothmann E. *et al.*, *SciPost Phys.*, **7** (2019) 034.
[22] Grazzini M., Kallweit S. and Wiesemann M., *Eur. Phys. J. C*, **78** (2018) 537.
[23] ATLAS Collaboration, *JINST*, **14** (2019) P12006.
[24] ATLAS Collaboration, *Eur. Phys. J. C*, **76** (2016) 292.
[25] Cacciari M., Salam G. P. and Soyez G., *JHEP*, **04** (2008) 063.
[26] ATLAS Collaboration, *Eur. Phys. J. C*, **77** (2017) 466.
[27] ATLAS Collaboration, *Eur. Phys. J. C*, **76** (2016) 581.
[28] ATLAS Collaboration, *Eur. Phys. J. C*, **79** (2019) 970.
[29] ATLAS Collaboration, *Eur. Phys. J. C*, **80** (2020) 528.
[30] Avoni G. *et al.*, *JINST*, **13** (2018) P07017.
[31] ATLAS Collaboration, *Eur. Phys. J. C*, **79** (2019) 639.
[32] ATLAS Collaboration, *Eur. Phys. J. C*, **81** (2021) 578.
[33] ATLAS Collaboration, *Phys. Rev. D*, **96** (2017) 072002.
[34] ATLAS Collaboration, Technical report, ATL-PHYS-PUB-2015-015 (2015) `https://cds.cern.ch/record/2037613`.
[35] ATLAS Collaboration (2022) `https://atlas.web.cern.ch/Atlas/GROUPS/PHYSICS/PLOTS/FTAG-2022-003/`.